

Optical Coherence Tomography: its role in the non-invasive structural examination and conservation of cultural heritage objects—a review

Piotr Targowski · Magdalena Iwanicka

Received: 5 April 2011 / Accepted: 7 November 2011 / Published online: 26 November 2011
© The Author(s) 2011. This article is published with open access at Springerlink.com

Abstract A brief introduction to Optical Coherence Tomography (OCT) is presented, stressing the origin of the tomographic signal and the detection methods defining various modalities of the technique. The parameters of the tomographs, such as axial and lateral resolution, wavelength and intensity of the probing light, imaging range, time of examination, and sensitivity are then defined, and a paradigm for interpreting the OCT tomograms provided. The second part of the article comprises a review of the utilisation of OCT for structural examination of artworks, illustrated with some representative results. Applications to the structural imaging of semi-transparent subsurface layers such as varnishes and glazes, of underdrawings and of reverse painting on glass, are described first, and then applications in the examination of the structure and state of preservation of historic glass, jade, glazed porcelain and faience are discussed. Finally, the use of OCT combined with LIBS analysis and laser ablation of surface layers is presented.

1 Fundamentals of the OCT technique

Optical Coherence Tomography (OCT) is a white light interferometric technique providing high resolution cross-sectional views (tomograms) of objects which moderately

absorb and scatter the probing light. Since it utilises light of low intensity, it is harmless to all known types of artworks. The examination is non-contact, fast, and does not require any preparation of the object examined. The resultant image has a convenient form, similar to the very popular photomicrographs of cross sections of samples collected from the objects. The technique is especially well suited to inspection of the internal structure of stratified objects because the in-depth (axial) resolution falls into the range of 1 to 10 μm , even though the lateral resolution is significantly lower, usually from 10 to 30 μm . The major constraint arises from the limited transparency of the strata of the object to the light used for examination. Nevertheless, the variety of objects to which the technique is being applied is still gradually increasing.

The OCT technique was invented in the mid-1990s by Huang et al. [1], and since then has become a well established diagnostic method in medicine [2], especially in ophthalmology. It is used mostly for imaging of human retinas in vivo through the iris of the eye, but also for examination of the geometry and diseases of the anterior chamber. Among other medical applications, utilisation in dermatology, oncology, gastrology, and gynaecology are especially important. At present, various commercial instruments dedicated to medical diagnostics are available at prices ranging from 50,000 to 80,000 Euros.

1.1 Principle of operation

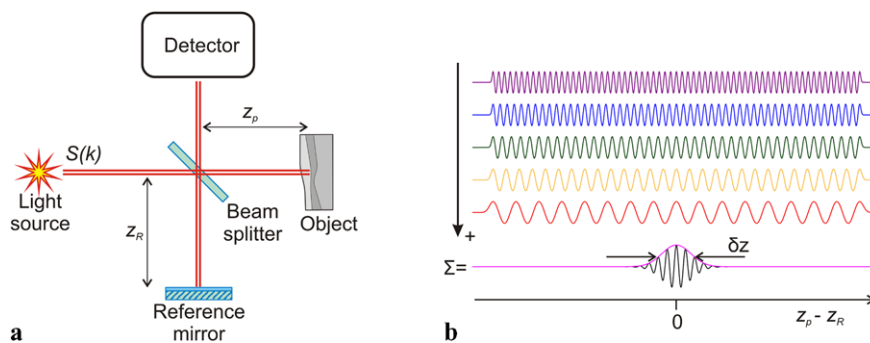
Omitting the technical details for simplicity, information on the internal structure of a suitable object is generated by interference between light reflected and/or scattered by details of its internal structure and the reference beam (Fig. 1a).

The intensity signal (see (1)) is proportional to the spectral density $S(k)$ of light emitted from the source, and may

P. Targowski (✉)
Institute of Physics, Nicolaus Copernicus University,
ul. Grudziądzka 5, 87-100 Toruń, Poland
e-mail: ptarg@fizyka.umk.pl

M. Iwanicka
Institute for the Study, Restoration and Conservation of Cultural
Heritage, Nicolaus Copernicus University, ul. Gagarina 7, 87-100
Toruń, Poland
e-mail: magiwani@gmail.com

Fig. 1 (a) Basic configuration of the OCT interferometer; (b) principle of TdOCT: multispectral interference produces a signal only for equal and close to equal paths in the arms of the interferometer



be expressed as a sum of four terms: the first two refer to the intensities collected directly from reference and object arms: α_p is the reflection/scattering coefficient of the p th layer of the object. It is assumed for simplicity that the reflection coefficient of the reference mirror is equal to 1; the 50:50 beam splitter is utilised to produce the interference. The third term represents mutual interference between signals from all layers of the object. It is relatively weak and usually falls below the noise level. The last term describes the interference between reference and object beams, and contains information utilised for OCT imaging. As can be seen, this signal oscillates with a frequency proportional to the product of the wavenumber k and the difference $(z_p - z_R)$ between the optical paths in the two arms.

$$\begin{aligned}
 I(k) = & \frac{1}{4} S(k) \left[1 + \sum_p \alpha_p \right. \\
 & + \sum_{\substack{p,q \\ p \neq q}} \sqrt{\alpha_p} \sqrt{\alpha_q} \cos[2k(z_p - z_q)] \\
 & \left. + \sum_p \sqrt{\alpha_p} \cos[2k(z_p - z_R)] \right]. \tag{1}
 \end{aligned}$$

There are two ways in which useful data can be extracted from this multispectral interference signal. Time-domain OCT (TdOCT) was developed first. In this variation of the technique, the signal is integrated at a detector, usually a photodiode, and the photocurrent is registered over time simultaneously with translation of the reference mirror. As can be seen from the simplified graph in Fig. 1b, due to the integration over a broad spectral range, the interference signal will not average to zero only if the optical path difference between the two arms of the interferometer is small. This range (δz in Fig. 1b) defines the axial resolution of the technique. Therefore, the amplitude of this signal for consecutive positions of the reference mirror carries information about the locations of scattering centres and/or reflective interfaces along the probing beam. This amplitude information is often referred to as an A-scan by analogy to ultrasonography, and when converted to intensities comprises

one vertical line of the tomogram. By parallel transference of the penetration beam to consecutive, adjacent positions, the whole image of the cross section (B-scan) is built up. The necessity of mechanically scanning the reference mirror forms a major drawback of the TdOCT technique: in spite of some advanced solutions utilising rapid scanning delay lines [3], TdOCT tomographs usually run more slowly than other types of OCT instruments. An interesting approach leading to elimination of this disadvantage is provided by Full-Field OCT, where 2D images are obtained with an interferometric objective of Linnik or Mireau type. Mechanical depth scanning is still necessary, but the whole 2D image is registered at a given depth with an image detector, and the mechanical limitations are less burdensome. By contrast with the previous approach, these images represent cross sections in planes parallel to the surface of the object. They are usually further combined into volume (3D) structural images. This makes it possible to obtain any arbitrarily chosen cross section during data post-processing.

The second approach to the structural information recovery is called Fourier-domain OCT (FdOCT). In the FdOCT instruments, the reference mirror is held in a steady position and the interference signal collected as a function of wavelength or wavenumber. This may be accomplished in two ways: in Spectral-domain OCT (SdOCT), a broadband light source is used together with a detector comprising a spectrograph equipped with a single-line CCD or CMOS camera; in Swept-Source OCT (SSOCT), a laser with rapidly scanned wavelength is used as the source, with a single photodiode as the detector. Both FdOCT modalities are available commercially or laboratory-made, and are able to scan with frequency range from 100 kHz to 1.4 MHz [4] over a broad range of wavelengths. The state-of-the-art of and prospects for very high speed OCT have been reviewed recently by Wojtkowski [5]. Whatever the method by which the signal is generated, it must be provided for further processing as a uniformly sampled function of wavenumber $k = 2\pi/\lambda$ (or optical frequency $\omega = kc$). The signal is then converted to z -space by numerical Fourier transformation, as directly follows from (1). The index m_p of a peak corresponding to a scattering centre positioned at optical distance z_p is thus

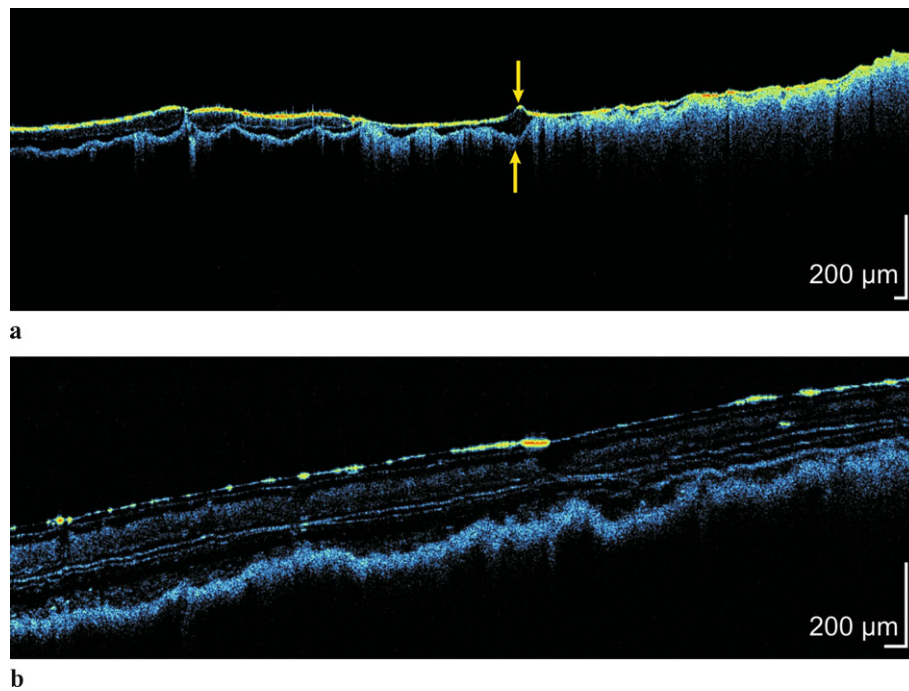


Fig. 2 Examples of OCT B-scans of two paintings on canvas. (a) Nineteenth-century oil painting with two layers of varnish; (b) multilayer structure of seventeenth-century painting with various layers of

glazes and varnishes. Both images were obtained with a SdOCT system of 3.5 µm axial resolution in air

given by:

$$m_p = \frac{1}{\pi}(k_{\max} - k_{\min})(z_p - z_R), \quad (2)$$

where k_{\max} and k_{\min} refer to the whole range of wavenumbers registered.

Since the envelope $S(k)$ of the interferometric signal is of arbitrary shape and finite range, the proper window, usually of Gaussian shape, must be applied to data before Fourier transformation. The resultant data represent a single A-scan, as before, but is obtained up to hundreds of times faster than with TdOCT. Additionally, due to the multidetector advantage, the SdOCT technique is significantly more sensitive than TdOCT [6].

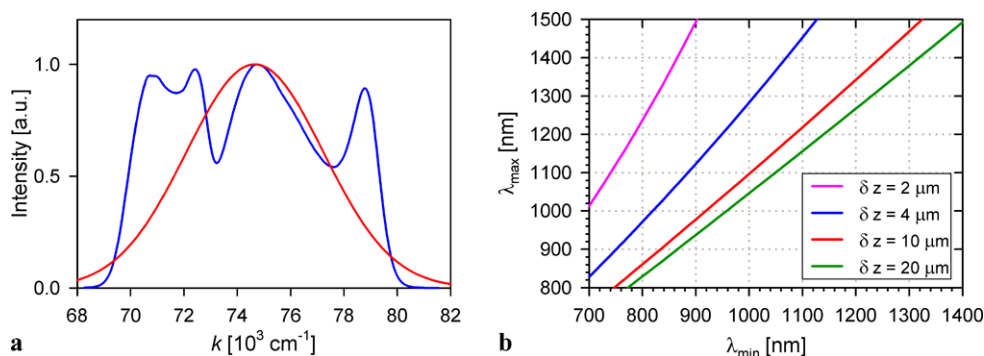
Results of the OCT examination (B-scans) are usually presented on a false colour scale (Fig. 2), where in areas from which no signal is detected (perfectly transparent or beyond the range of penetration) remain black, whereas areas which weakly scatter or reflect the probing beam are shown in cold colours (from blue to green), while those highly scattering or reflecting are represented by warm colours (from yellow to red). Light usually approaches from the top: in Fig. 2, the first strong line is thus the air-to-varnish boundary. Below this, some semi-transparent layers are visible: in the simple case illustrated in Fig. 2a, there are two layers of varnish (in the left-hand-side region), in Fig. 2b exact characteristics of these layers need further ex-

amination. The figure also illustrates a common way of presenting the results: with the vertical scale elongated for better readability due to the difference in axial and lateral resolution (as already indicated, the axial resolution is much higher). Additionally, one must remember that the depths recovered from (1) represent optical distances. Correction procedures may be applied to recover geometrical distances (see Fig. 5 in [7]), but if the layers examined are reasonably flat, a simple vertical scale recalculation is sufficient. However, in the case of the lump of varnish appearing in Fig. 2a (see arrow), the distortion of the layer underneath is significant, and it is necessary to be aware of this artefact.

Sometimes different intensity scales are used: simple monochrome (see Fig. 4 and Fig. 8f in Sect. 2, where the strongly scattering structures are registered in white), or sometimes more readable reverse grey scale (see Fig. 5 in Sect. 2 and, e.g., Fig. 4 in [8]) with non-scattering regions shown in white and strongly scattering ones in black.

It must be emphasised that various instrumental solutions have specific advantages and disadvantages. There is therefore no universal answer to the question as to the best OCT system. The choice should be made in the context of performance parameters. The information provided in the following chapters is intended to serve as a guide and encouragement to further reading on selection of the most relevant system in any particular case.

Fig. 3 (a) An example of the spectrum of the light source used in high resolution OCT (D855 from Superlum, Ireland, blue line) and a Gaussian function used in the shaping procedure leading to the best axial resolution available with this source; (b) an estimation of axial resolution in air (4) available from sources emitting in various ranges of wavelengths



1.2 Parameters of the OCT instruments

Axial resolution δz is a parameter which is usually considered crucial for OCT systems. It depends on the spectral width Δk_{FWHM} of the light source, and in air may be estimated by the formulas:

$$\delta z = \frac{4 \ln 2}{\Delta k_{FWHM}} \quad \text{or} \quad \delta z = \frac{2 \ln 2}{\pi} \frac{\lambda_{centr}^2}{\Delta \lambda_{FWHM}}. \quad (3)$$

However, it should be admitted that the full-width-at-half-maximum (FWHM) parameter is only well defined for sources with a single dominating emission band. The very broadband sources presently used in OCT have spectral envelopes very different from Gaussian (Fig. 3a, blue line). Therefore, as was mentioned in the previous chapter, a certain shaping procedure [9] must be adopted and, especially in case of FdOCT systems, the axial resolution should rather be estimated by:

$$\delta z = \frac{1}{n_R} \frac{8 \ln 2}{k_{max} - k_{min}} \quad \text{or} \quad \delta z = \frac{1}{n_R} \frac{4 \ln 2}{\pi} \frac{\lambda_{max} \lambda_{min}}{\lambda_{max} - \lambda_{min}}, \quad (4)$$

where the indices max and min refer to the whole range of the light source, and it is assumed that the total bandwidth of the source is approximately twofold broader than its FWHM after shaping. In Fig. 3a this equivalent spectrum is shown in red. Equation (4) additionally contains the factor $1/n_R$, which accounts for the increase of effective axial resolution in media of (group) refractive index n_R . It is due to the fact that the depths represented in (3) and (4) are optical ones.

As may be noticed from Fig. 1b, the axial resolution δz is lower than available from phase-sensitive methods, in which it is a fraction of the wavelength of the monochromatic light source, but here the position of the structure within the object examined is retrieved unequivocally, without the disadvantage of phase ambiguity. It is also clear from the formulas of (3) that, for light sources of given bandwidths (in nm), the resolution decreases as the central wavelength increases. This is unfortunate, since the transparency of many media increases with the wavelength of examination. The bandwidth of light sources used in OCT varies from 20 to

200 nm in the spectral range of 700 to 1500 nm, which leads to axial resolution of 2.0 to 20 μm (Fig. 3b) in air. Only some Full-Field OCT systems utilising visible light have axial resolution better than 1 μm .

Lateral (in-plane) resolution in OCT is defined entirely by the properties of the optics of the object arm of the interferometer. In the majority of OCT systems, utilising the scanning beam to examine the structure of the object, it may be derived (by searching for spots separation similar to Raileigh’s criterion for Airy’s discs) from the waist w_0 of the Gaussian beam focussed at the object examined:

$$\delta x = \sqrt{2} w_0 = \frac{2\sqrt{2} \lambda_{center}}{\pi} \frac{f}{\Phi}, \quad (5)$$

where f is the focal length of the objective and Φ is the diameter of the probing beam at this lens. Due to technical limitations for scanners used in the object head, it is difficult to work with beams of diameters greater than a few millimetres. As a result, lateral resolution usually falls into the range of 15 to 40 μm and is much lower than the axial one. This makes the OCT technique especially well suited for examination of stratified objects, for which the axial resolution is decisive for proper interpretation of the images obtained. As is also seen from (3) and (5), in contrast with confocal microscopy, axial and lateral resolutions are fully decoupled in OCT.

It is obvious that neither resolution depends on the modality of the OCT system. This is not the case for other important parameters: central wavelength, imaging range, time of examination, and sensitivity.

The central wavelength of the radiation utilised determines the choice of available detectors: for instruments working at wavelengths below 1 μm , both high resolution CCD/CMOS cameras and photodiodes are easily available. Therefore, any of the TdOCT, SdOCT and SSOCT systems may be employed. For longer wavelengths—up to 1.7 μm —line scan InGaAs cameras (Goodrich ISR Systems, Princeton, USA) have lately become available and made it possible to develop SdOCT systems for this spectral range, also. At present, however, this longer-wavelength range is

explored mostly by means of swept source (SSOCT) systems. In order to ensure high sensitivity of the instrument, the light source must also simultaneously have high spatial coherence. Most convenient are broadband single-mode fibre sources, but these are available only for wavelengths above 700 nm.

The *imaging range* of an OCT instrument is defined as the axial range which may be examined and then presented in a single tomogram. In the case of TdOCT, the only limitation on this arises from the depth of focus (DOF) of the probing beam:

$$\text{DOF} = \frac{8\lambda_{\text{center}}}{\pi} \left(\frac{f}{\Phi} \right)^2 \quad \text{or} \quad \text{DOF} = \pi \frac{\delta x^2}{\lambda_{\text{center}}}. \quad (6)$$

The DOF is defined as the range within which the lateral resolution deteriorates by a factor of $\sqrt{2}$. However, it is possible to overcome this limitation by simultaneous translation of the focussing lens and the reference mirror [10].

The same formulas, (6), hold for other OCT modalities, but there are also other specific factors further limiting the imaging range. In the case of FdOCT, an additional limitation is met in the procedure for recovery of the OCT data from the interferometric intensity signal. Therefore, the imaging range may be derived from (2) using the Nyquist limit. Since in standard FdOCT instruments the phase of the signal is not registered, the data $I(k)$ in (1), which undergoes Fourier transformation, is real. The resulting function is therefore symmetric about zero optical distance difference, and two symmetric images are retrieved. In this way, only half of the imaging range may be effectively utilised. This liability was for a long time regarded as a major limitation of the SdOCT technique. However, many methods for suppression of one of the mirror images are now known, permitting the utilisation of the whole imaging range. These are usually at the cost of a minor increase in the complexity of the setup, together with a two- to five-fold increase of examination time. Nevertheless, in the majority of cases it is sufficient to use just one side of the imaging range. In that case, the Nyquist theorem gives:

$$z_{\text{max}} = \frac{\pi}{(k_{\text{max}} - k_{\text{min}})} \frac{N}{2} \approx 0.28N\delta z, \quad (7)$$

where N is the number of pixels of the camera utilised in the spectrograph. A more fundamental description of the decay in sensitivity with depth has been derived by Woods and Podoleanu [11] using a limited wave-train model.

A limitation similar to that of (7) holds also for SSOCT systems, but there N may be as high as 10^5 and a much greater imaging depth may be expected. In that case, the fundamental constraint derives from the spectral width of the laser line δk_{FWHM} :

$$z_{\text{max}} = 0.8 \frac{1}{\delta k_{\text{FWHM}}} \sqrt{\rho}, \quad (8)$$

where ρ (in dB) denotes the acceptable decrease of intensity of the OCT signal. Additionally, the bandwidth of the photodiode can be a limiting factor for detecting the high frequencies of the interference signal encoding deeply buried structures. Nevertheless, SSOCT usually provides much greater imaging depths than does SdOCT.

The *time of examination* is an important factor, especially in diagnostic medicine, which—if short—reduces motion artefacts and increases patient comfort. In the case of examination of artworks, it is also very convenient to keep it short, since this helps in quickly selecting interesting areas for examination, which makes working with OCT highly effective, and renders possible the utilisation of OCT for real-time control of conservation treatments.

The *sensitivity* of OCT tomographs is defined by the maximum attenuation of the probing light within the examined object which still leaves it detectable. Here, spectral domain OCT offers a significant advantage over the single-detector methods. This parameter is especially important in the investigation of samples exhibiting some degree of IR absorbance, such as glazes and other paint layers.

The *power of the probing beam* must be considered carefully to ensure that there is no possibility of damage to the object under examination. Generally, very low intensities of light are used in OCT: due to the high sensitivity of the detection system, high intensities are also impractical because they lead to image artefacts caused by saturation of the detector (vertical smears in Fig. 6). Usually the radiation power at the surface of the object is below 2 mW. In such a case, for a typical SdOCT system with an acquisition time of 30 μs for an A-scan and a lateral resolution of 20 μm , the fluence of the infrared radiation may be estimated to be 10 mJ/cm^2 , far below the damage threshold. It is worthwhile underlining the fact that such intensities are also within the ANSI safety limit for examination of the human retina [12].

Typical parameters for various OCT systems are collated in Table 1. It must be emphasised that the data given in the table represent average figures, compiled from many instruments of typical construction, and should not be associated with any particular implementation.

As follows from this short overview of the properties of various OCT systems, at its present stage of development this technique offers many solutions. The future user should carefully choose the modality best fitting their application. In Table 2, the major advantages and disadvantages of the main OCT systems are briefly summarised.

1.3 OCT systems used for examination of cultural heritage objects

Many OCT systems designed for medical diagnostics may be used for examination of art objects. The only significant limitation originates in the optics of the object arm: instruments for retinal examination have to be excluded due to the

Table 1 Typical parameters of various OCT systems

	TdOCT (translated mirror)	Full-Field OCT	SdOCT (2048 CCD spectro- graph)	SSOCT (FDML laser)
Available central Wavelength	700–1500 nm	400–1300 nm	700–1500 nm	1100–1500 nm
Imaging depth	<20 mm	0.5 mm	2 mm	<15 mm
Examination rate	200 A-scan/s	1 slice/s	25 000 A-scans/s	300 000 A-scans/s
Sensitivity	80 dB	<85 dB	100 dB	100 dB

Table 2 Major features of main OCT modalities

	TdOCT	SdOCT	SSOCT
<i>Advantages</i>	Unlimited depth of imaging	Fast acquisition (possible 3D imaging)	Very fast acquisition
	Simple basic design	High S/N	Adjustable resolution and depth of imaging High S/N
<i>Disadvantages</i>	Slow acquisition	Limited depth of maging	Light sources still under development
	Moving parts in delay line	Sensitive to specular reflections	Sensitive to specular reflections
	Artefacts (side lobes) for non-Gaussian source difficult to remove	Wavelength of operation limited by CCD camera	

specific optics designed for observation through the cornea and the lens of the eye, so that these systems can produce sharp images of the retina, but are unsuitable for other applications. Other current medical, as well as general-purpose commercial product, systems may be used without significant modifications.

When choosing the OCT system for examination of art, its flexibility in terms of coping with a variety of such objects should be taken into account: the art work may be of various sizes or thickness, and sometimes may be examined only in specific (e.g. vertical or horizontal) position. Very often the examination must be performed in situ. Therefore portable instruments are preferred.

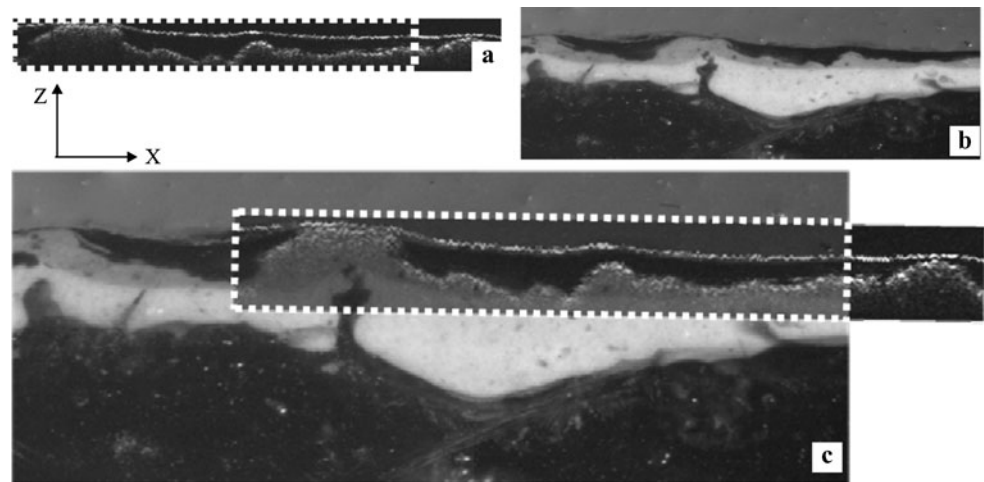
Since a large range of practical solutions are usually described in detail in original papers, the authors of this review feel released from the obligation to repeat this information here. Taking note of our overview of the important parameters given above, the reader is directed to these publications. Among those devoted to examination of cultural heritage objects, the most comprehensive description of TdOCT instruments may be found in [13–17], of SdOCT systems in [7, 18], and of SSOCT in [17, 19–21]. Solutions for Full-Field OCT with the Mireau interferometer are discussed in [22–24], and with the Linnik configuration of a Michelson interferometer in [25]. In addition, a polarisation-sensitive TdOCT tomography, in an application to the examination of parchment, is described in [26].

In addition to the general descriptions referred to above, some specific issues are addressed: in paper [27] by Hughes et al., an interesting method for the reduction of speckle noise is presented. An important matter—beyond the scope of this paper, however—is the continuing search for new methods of processing and presentation of data. Two papers by Sylwestrzak et al. fall into this category: in [28] new formats of presentation of 3D data are described, and in [29] the modern technique of ultra-fast massively parallel processing of OCT data is presented.

2 Applications to examination of the structure of artwork

The first internationally available reports on the use of the OCT technique for artwork analysis are from 2004 by Yang et al. [13], Targowski et al. [41], and Liang et al. [30]. In these early papers, the major fields of interest were already recognised: examination of varnish and glaze layers of paintings and semi-transparent solids such as jades and glazed ceramics. Additionally Yang et al. pointed out the application of OCT for assessment of possible forgeries of

Fig. 4 Direct comparison of the OCT image (a $280\ \mu\text{m} \times 2\ \text{mm}$) with the cross-sectional photomicrograph (b). In (c), superposition of these two images is shown. Reproduced from [15] with permission



jade items. Up to the present (March 2011), over 60 papers [31] have been published on the OCT examination of artworks.

2.1 Examination of the structure and state of preservation of paintings

This application is straightforward, and from its very beginning was considered an alternative to sampling. Arecchi et al. [15, 32] have proved by direct comparison that the OCT tomogram of the varnish and glaze layer is equivalent to a cross-sectional photomicrograph of the sample taken in the same place.

Liang et al. [14] first pointed out what is probably the most important advantage of the OCT sectioning over sampling collection: the number of samples and the location of their collection are strictly limited by conservation ethics mostly to areas of existing damage. Since the OCT technique is non-invasive, the examination may be repeated as many times as necessary in any desirable place, so that results obtained with this technique may be considered more representative.

A major concern at the initial stages of development of this technique is centred on its applicability to investigation of the paint layer, due to the limited transparency of such strata to the radiation used. This limitation remains valid, but increasing instrumental sensitivity, together with improved understanding of the images obtained, has rendered it less significant. The only systematic studies on the applicability of OCT to the imaging of paint layers composed of various pigments were performed by Szkulmowska et al. [33]. They analysed 47 different commercially available oil paints with two OCT systems working at extreme central wavelengths: 0.83 and 1.55 μm . As expected, better results were obtained with the longer wavelength observation: for that case, 16 of the 47 pigments qualified as having high transparency, while

a further 6 were of medium transparency. For 0.83 μm observation, 9 of the 47 fell into the first category, a further 7 into the second. However, as can be seen from (3), increasing the wavelength of light used for examination leads to rapid deterioration of the axial resolution. This trade-off must therefore always be taken into account when new experiments are under consideration. An important account of this subject has also been presented by Liang et al. [34].

When a varnish or similar layer is under investigation, the choice is rather simple: short wavelengths are preferred to ensure high resolution. Superb axial (1.5 μm) and lateral (1.0 μm) resolutions were reported by Latour et al. with the use of red (visible) light and a Full-Field TdOCT system with Mireau objective for examination of pigmented lacquers on slabs [22] and of the coatings on an historic violin [24]. However, a disadvantage of microscope system used lies in the limited lateral field of view. Examination of the stratigraphy of the varnish layers with OCT was successfully executed by Targowski et al. [18] for analysis of the locations of paint layers involved in inscriptions in relation to other strata: two paintings were analysed at the request of the conservation studio. In the first case, it proved possible to resolve some doubts concerning the history of the painting. In the second case, evidence of forgery of the signature was uncovered. Processes occurring during drying of the varnish layer were investigated by Liang et al. [35]. They pointed out that the varnish Paraloid B-72, when drying, begins to follow the roughness of the substrate. This may be used as a non-contact method of determination of the stage of the drying process. The ability of the varnish layer to either reproduce or level the roughness of the surface of underlying paint (depending on molecular weight of the resin) was further investigated by Targowski et al. [7] and found to be in accordance with the pre-OCT conclusions derived much earlier by de la Rie [36].

The advantage of coherent detection in OCT was utilised by Liang et al. [14, 34, 35, 37, 38] and by Adler et al. [19] for

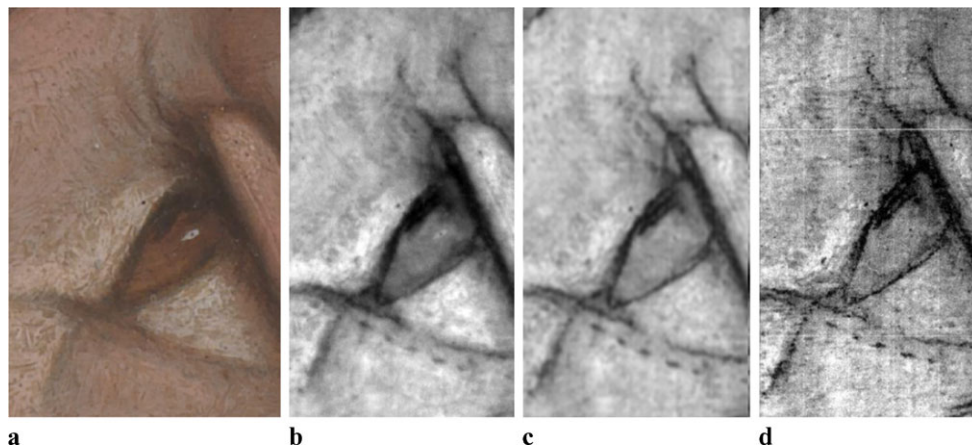


Fig. 5 (a) The Virgin and Child with an Angel (NG 3927), after Francesco Francia, probably second half of the 19th century, detail of the angel's eye, photo © The National Gallery, London; (b) infrared image of the same region obtained using a CCD camera through a bandpass filter at 880 nm; (c) result of examination in range 900–

1700 nm with SIRIS camera equipped with InGaAs sensor, image ©The National Gallery, London; (d) en-face OCT image at 930 nm (median of 40 en-face images); the size of the area under examination is 10 by 15 mm. Reproduced from [37] with permission

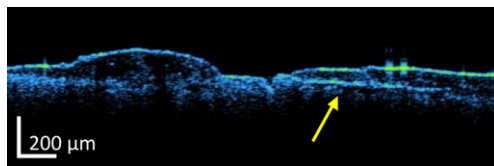


Fig. 6 A delamination (arrow) extending under the varnish layer from the damage localised in the centre of the tomogram. Reproduced from [39] with open access

imaging underdrawings covered entirely by the paint layer. The en-face TdOCT modality is especially well suited to this application. Comparison with images obtained with infrared reflectography shows up the higher contrast of images obtained with OCT (Fig. 5). Both techniques use radiation of similar wavelength to ensure sufficient penetration, but the non-coherent reflectograms are always blurred somewhat by scattering and/or refraction of penetrating light in the paint layers covering the drawing through which it must propagate twice. Since in this OCT experiment the signal is integrated only over the thin layer of the underdrawing, all unwanted noise is rejected by the coherence gate, and so does not contribute to the interference nor therefore propagate into the resultant image. However, a minor disadvantage of using OCT for this task should be noted: it lies in the limited field of imaging with this technique, and thus it is mostly appropriate only for examination of small details. This kind of analysis was performed by Adler [19] for en-face imaging of punch-marks in gold, covered by a thick layer of varnish. Again, by discrimination against signal from overlaying structures, very sharp and detailed images of the punch-marks were obtained, permitting identification of the craftsman's tool.

A case study presented by Rouba et al. [39] may serve as an example of OCT evaluation of the state of an artwork's preservation. The OCT tomogram was taken from an area of surface abrasion in a historic oil painting. It is evident that, in addition to the surface damage, a delamination at the boundary between the thick varnish layer and the underneath glaze layer is present (arrow in Fig. 6). It is not possible that this crack could have been detected with standard en-face observation by light stereomicroscope.

A specific application of OCT incorporating examination of paintings and of glass (to be discussed in the next paragraph) is the inspection of reverse paintings on glass (*Hintergemalerei*), [40], where the paint layer is under investigation but accessed through the transparent sheet of glass. This kind of folk art was popular in Central Europe until the mid-20th century, and is characterised by reverse order of the painting process. Since the picture is intended to be viewed through the glass, the paint layers decisive for the visual effect are directly adjacent to the glass support. This renders them inaccessible to physical inspection, and the advantage of using OCT for this task, developed by Iwanicka et al. [8, 41], is irrefutable. Apart from mere detection of various stages of formation of blisters between the glass and the paint layer, the results of filling them with consolidation adhesives during previous conservation treatment were also evaluated. In addition, areas of early delamination can also be localised in the OCT tomogram, as lines of strong reflection of light caused by a high gradient of refractive index in the delaminating area (1b in Fig. 7). A similar application of OCT is the examination of a painted photograph, part of a collage, glued face-down to a sheet of glass [41]. However, in this case, for technological reasons, both the glass and the glue layer had been damaged.

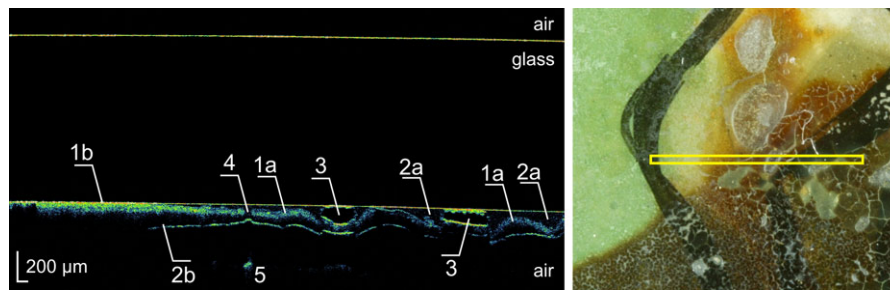
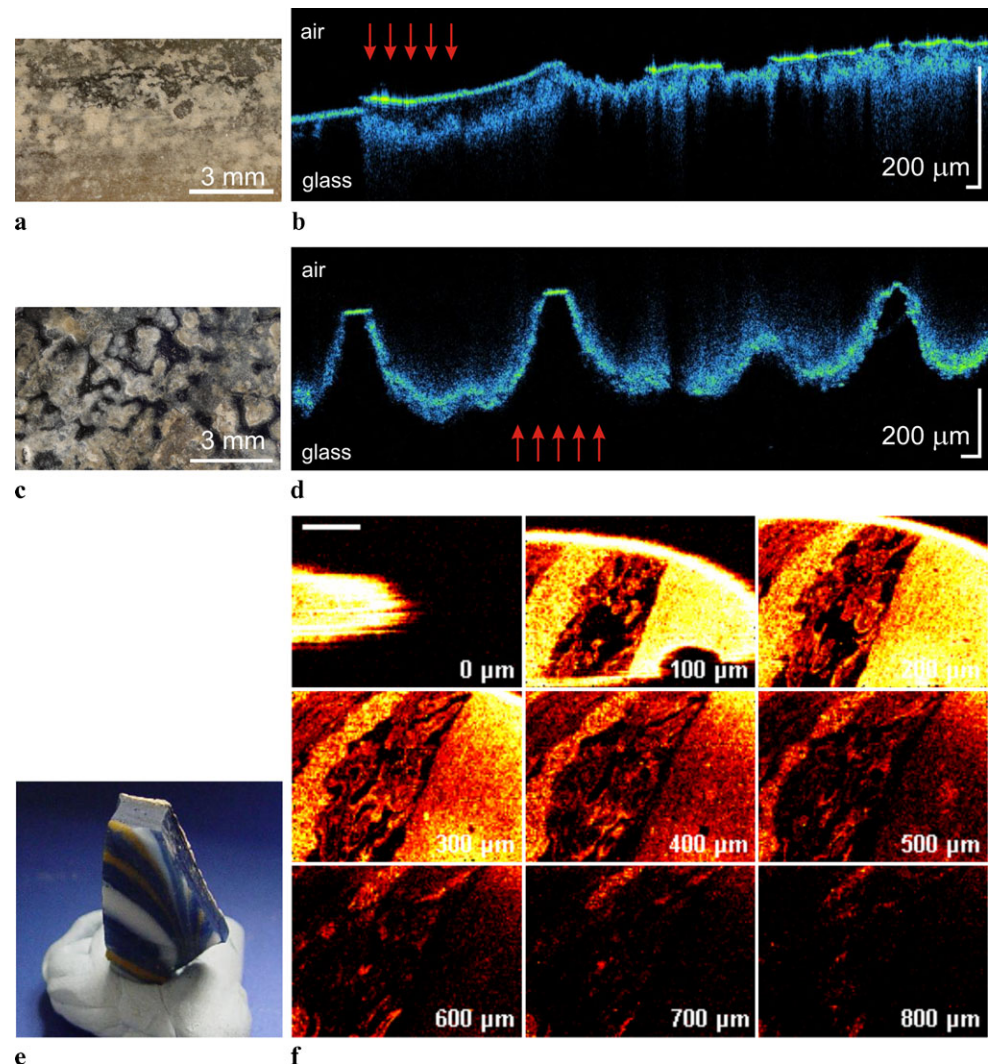


Fig. 7 Example tomogram revealing destruction in a *Hinterglas-malerei*. 1: original paint layer detached (1a) and delaminated (1b) from the glass; 2: consolidation adhesive, partially filling the detachments (2a) or covering the reverse side of the paint layer (2b); 3: air

bubble within the consolidant; 4: crack in the paint layer, filled with the consolidant, passing probing light which thus penetrates through to the backing paper (5)

Fig. 8 OCT tomograms of historic glass: (a–d) samples of fourteenth-century glass, Basilica of St. Mary, Cracow, reproduced from [41] with permission. (a) Yellow glass, inner side of window—delamination of glass surface; (b) OCT tomogram of sample (a) scanned from the inner side; (c) blue glass, outer side of window—pitting; (d) OCT tomogram of sample (c) scanned through glass from the inner side. *Arrows* indicate the direction of illumination by the OCT probing beam; (e–f) Egyptian core-formed glass sample (British Museum, No. 36458), reproduced from [17] with permission—Full-Field OCT slices of Egyptian core-formed glass at 100-µm depth intervals. The 3D structure of the coloured glass layers can be observed. The scale bar is 2 mm



2.2 Examination of the structure and state of preservation of historic glass

There are two main reasons for using OCT in the examination of historic glass. First of all, glass is usually trans-

parent enough to permit deep penetration of the examining light. Furthermore, if a glass sheet is considered, it is frequently possible to examine details of one of its sides from the other side, with light penetrating through its whole thickness. This is sometimes convenient for layers of strongly ab-

sorbing coloured glass [42], or for inspection of the highly scattering gel layer formed at the glass surface due to atmospheric corrosion. If such deterioration is examined with light approaching directly from the damaged side of the glass (Fig. 8b), the thickness of the gel layer may be overestimated due to multiple scattering of light inside it. This well-known artefact of OCT imaging manifests itself in the form of fading “tails” below the last-imaged structure. If the corrosion layer is examined through the glass (Fig. 8d), the direction of these “tails” reverses, and the gel–glass boundary is clearly visible.

The suitability of OCT for imaging corrosion layers of stained glass was confirmed by Kunicki-Goldfinger et al. [43] by comparison with SEM (Scanning Electron Microscopy)-BSE (Back Scattered Electrons) images of a cross section of the same sample. The SEM-BSE technique is commonly used for detection of the build-up of the silica-rich gel layer at the glass surface during the corrosion process. However, in order to employ the SEM-BSE method, it is necessary to prepare a polished cross section of the sample. Therefore, this method, although not destructive of the sample, may be used in limited cases only. OCT offers here an interesting alternative, since it is truly non-invasive and may be used at any point of the glass sheet, in principle even without dismantling the window. Similar results, but obtained with a 1300 nm system, have been reported by Hughes [17].

Some of the ancient glass artefacts from the collections of the British Museum have been examined by Liang et al. [17, 34, 37]. These studies confirmed the ability of OCT to reveal details of the internal structure of the glasses up to 0.5 mm under the surface. The usefulness of OCT for fast screening of museum collections may be important also in diagnosing crizzling of glass (see Fig. 1 in [43]). This phenomenon is a deficiency of glass caused by imbalance in the ingredients of the batch, and can be recognised as a network of fine cracks, very often developing with time and possibly leading eventually to the total destruction of the object.

An OCT investigation [41] of such samples revealed that the crizzled layer is of uniform, though not the same, thickness on both sides of the same sheet.

2.3 Examination of the structure and state of preservation of other semi-transparent objects

Among other objects, artefacts made of jade have been investigated, first by Yang et al. [13], later by Liang et al. [37], and recently by Chang et al. [21]. Yang showed, by comparing a sample of ancient jade before and after artificial ageing (by burning with a gas torch), that it is in principle possible to distinguish between them using OCT. The artificial ageing induces some small-scale alterations to the structure of the sample leaving large-scale features unchanged, making

the overall structure more heterogeneous. The original ancient pieces have a fairly uniform structure as a result of the simultaneous formation of small-scale scattering centres (these are responsible for the whitening of jade) and consequent diminishing of the large-scale features. Such observation may help in recognition of possible frauds. This idea of using OCT for assessing the quality and authenticity of jade was developed further by Chang et al. [21]. However, in contrast with the work previously referred to, these authors provided a quantitative texture analysis method based on six well-defined parameters which may be derived from the OCT signal and further combined into a 6-D texture vector. The length of this vector, together with the reflecting properties of the jade surface, may be used for differentiation among various types of jades.

Another group of objects examined with OCT from the very beginning are those made of porcelain and faience [17, 37, 41]. The most comprehensive study was made by Yang et al. [16], examining various items of 10th–14th century Chinese glazed ceramic shards. Major attention was paid to the ability of OCT to recognise different phases and phase boundaries within the glaze layer. The information acquired by the OCT examination may be used for identification of the manufacturer of the porcelain, and detection of some glaze flaws such as impurities and internal cracks.

Finally, some less extensive studies on painted enamel on a ceramic tile were performed by Liang et al. [37], and on parchment samples by Góra et al. [26].

2.4 OCT as a supporting tool for LIBS stratigraphy

Laser Induced Breakdown Spectroscopy (LIBS, or sometimes LIPS) is a micro-invasive analytic technique used in materials science mostly for examining the elemental composition of metal alloys. This is determined by analysis of the spectrum of atomic fluorescence emitted from the small plasma plume generated by a short, high-power laser pulse focussed on or into the material examined. Since the diameter of the crater formed during the LIBS analysis does not usually exceed 100 μm , the invasiveness of this technique is limited, and it is often used for examination of objects of cultural heritage. A comprehensive review of this application has been presented by Fotakis et al. [44]. A very important variety of this application is LIBS stratigraphy, where the ablation crater is hollowed out gradually by a sequence of laser pulses. Since the fluorescence spectrum is registered after each laser pulse, the concentrations of elements detected may be determined as a function of the laser pulse number. This gives some indication of the depth dispersion of elements contained in the object examined. A significant drawback of this approach lies in the lack of information on the exact depths of the crater after each pulse. This is especially important, since the ablation rate may be significantly different for each layer of the object. The solution

lies in monitoring the depth of the ablation crater after every laser pulse. To the best of our knowledge, the first time the idea of integrating white light interferometry with LIBS for this purpose appeared in its inclusion in the patent granted to Detalle et al. [45] and described in the paper by Dufour et al. [46]. In 2004, Papazoglou et al. [47] presented a LIBS apparatus comprising a white light interferometer, similar to a Full-Field TdOCT system, for use in examination of cultural heritage objects. This instrumental solution was illustrated by some results of employing it in elemental depth profiling of a daguerreotype. Due to the high axial resolution of their interferometer, the authors were able to determine the thickness of the gold-enriched covering layer to be 1.7 μm . Another study on the elemental composition of a metal object was performed by Amaral et al. [48]. Using a commercial TdOCT system (6- μm axial and lateral resolutions) and a Calibration-Free LIBS method, they were able to trace the percentage concentrations of various elements (mostly metals) in historic Brazilian coins for 20- μm depth steps. It is worth noting that, since the structure of the coins was rather homogeneous, it was not necessary to profile the crater after each laser pulse—that was measured after completion of the sequence of pulses, and depth data for each pulse was interpolated. Preliminary results on using a LIBS-OCT system to determine the stratigraphy of pigmented layers of paintings were presented by Kwiatkowska et al. both for a model [49] and for a historic painting [50]. In both cases, it was confirmed that it is possible to re-calibrate the depth scale of LIBS concentration profiles with the aid of OCT. Since the ablation rate varied from layer to layer, the dependence of crater depth on pulse number was not linear. Furthermore, changes in the crater ablation rate, determined from the depth-pulse relationship, are very helpful in recognising the boundaries between consecutive strata in the paint layer. Additionally, an OCT tomogram registered before the LIBS experiment, exactly in the same place, permits conscious choice of the best location to examine, helping with avoidance of ambiguous areas such as those of previous conservation treatments.

2.5 Prospective application of OCT as a supporting tool for laser ablation cleaning

This specific, and still only prospective, application has been developed exclusively by our group since 2007 in close cooperation with the Institute of Optoelectronics of The Military University in Warsaw, Poland. Attempts to remove varnish and similar coatings by means of laser ablation have their own long history, beyond the scope of this contribution. Briefly: varnish layers should be removed if they suffer from discolouration or loss of transparency due to prolonged exposure to light and/or external pollutants. Although, traditionally, varnishes are either removed mechanically with a

scalpel, or chemically with solvent mixtures, or by using a combination of both methods, in cases of very firm or hardly soluble layers this approach is extremely difficult, and endangers the paint layer underneath. In such cases, laser ablation may be considered an interesting possible alternative. However, possible damage to the underlying strata is a major concern, since they are at least similarly vulnerable to laser ablation. In contrast with the well-established stone-cleaning treatment, where the process usually terminates automatically when, after removal of the strongly absorbing contamination layer, the white well-reflecting stone surface is reached, the laser-ablation process of varnish removal is not self-terminated. It is therefore necessary to introduce a specific controlling mechanism into this procedure. About ten years ago, an automated workstation was developed [51] in which the LIBS technique was employed to control the termination of varnish removal by detecting spectral lines from paint pigments in the ablated plasma. Obviously however, this technique does not allow control of mere thinning of the varnish layer rather than its complete removal.

On the other hand, it seems that OCT may be employed here as an alternative monitoring system, since the varnish is usually transparent enough to be imaged through the whole of its depth. Up to now, experiments have been conducted with three groups of varnishes (dammar, ketone, and acrylic), employing different lasers operating both in the far infrared ($\lambda = 2.936 \mu\text{m}$) [42, 52] and in the UV ($\lambda = 0.266 \mu\text{m}$) [53, 54]. Depending on the laser/varnish combination, OCT enabled the distinction of three processes caused by laser radiation: true ablation of the varnish layer, its exfoliation, and its melting. However, the majority of these results, apart from those announced by Góra et al. [53] (electronic version [55]), were not obtained in real time. Instead, raw data were collected to the hard disc of a suitable computer, then post-processed in order to obtain the OCT images. In the case of the experiment described in the publications by Góra et al., real-time results were shown, but the image quality was rather poor. To summarise, for successful monitoring of laser ablation by means of OCT, two conditions have to be fulfilled: the system must operate with as high in-depth resolution as possible, and very fast data processing must be employed. As the next stage of development, one may consider monitoring the ablation process by automatic recognition of the thickness of remaining layer of varnish together with appropriate control of the laser pulse frequency.

3 Conclusions

As may be gleaned from this short review, applications of OCT in conservation–restoration practice fall into two categories: inventory techniques aiding in revealing structural

information, and tools assisting in the optimal performance of other analyses and treatments.

As was also shown above, a major limitation arises from the limited transparency of many of the constituents of art objects. However in many such objects, the intended visual effect is built up by the combined perception of many sub-surface layers, as in paintings with glazes and varnishes. These layers must thus be at least semi-transparent, and are therefore accessible to examination by OCT.

When OCT is used for structural analysis, it is important to note that, although it is characterised by superb in-depth resolution, it is sometimes difficult to interpret the composition of the layers imaged (Fig. 2b). The most promising possible resolution of this problem seems to be that of combining OCT with other non-invasive techniques such as multispectral imaging, XRF, and Raman analysis, or using it in cases when the general structure of the object is known, but the local thickness and condition of layers need to be revealed in as many locations as possible.

Another direction for the future development of the technique, leading directly to practical applications, is, in our opinion, further advance in post-processing of OCT images for the automatic recognition of strata in the object under investigation, possibly simultaneously revealing some information about its properties. The rapid growth of medical applications of OCT, especially in terms of image quality and the understanding of its content, leads us to believe that the applications of OCT in the area of cultural heritage will also make further significant progress in the coming years.

Acknowledgements Financial support was provided by the Polish Government through research grants for 2009–2011. The research leading to these results was partly funded by the EU Community's FP7 Research Infrastructures Programme under the CHARISMA Project (Grant Agreement 228330). The publication reflects only the author's views and the Community is not liable for any use that may be made of the information contained therein. Neither the CHARISMA consortium as a whole, nor a certain participant of the CHARISMA consortium, warrant that the information contained in this document is capable of use, nor that use of the information is free from risk, and accepts no liability for loss or damage suffered by any person using this information. MI gratefully acknowledges support from the VENTURES programme of the Foundation for Polish Science co-financed by the Innovative Economy Operational Programme within the European Regional Development Fund. The authors would like to thank Dr Michalina Góra for valuable discussions, especially regarding parameters of the OCT systems, and Dr Robert Dale for critical reading of the manuscript.

Open Access This article is distributed under the terms of the Creative Commons Attribution Noncommercial License which permits any noncommercial use, distribution, and reproduction in any medium, provided the original author(s) and source are credited.

References

1. D. Huang, E.A. Swanson, C.P. Lin, J.S. Schuman, W.G. Stinson, W. Chang, M.R. Hee, T. Flotte, K. Gregory, C.A. Puliafito, J.G. Fujimoto, *Science* **254**, 1178 (1991)
2. W. Drexler, J.G. Fujimoto, *Optical Coherence Tomography. Technology and Applications* (Springer, Berlin, 2008)
3. A.M. Rollins, J.A. Izatt, in *Handbook of Optical Coherence Tomography*, ed. by B.E. Bouma, G.J. Tearney (Marcel Dekker, New York, Basel, 2002), p. 99
4. T. Klein, W. Wieser, C.M. Eigenwillig, B.R. Biedermann, R. Huber, *Opt. Express* **19**, 3044 (2011). doi:[10.1364/OE.19.003044](https://doi.org/10.1364/OE.19.003044)
5. M. Wojtkowski, *Appl. Opt.* **49**, D30 (2010). doi:[10.1364/AO.49.000D30](https://doi.org/10.1364/AO.49.000D30)
6. R. Leitgeb, C.K. Hitzenberger, A.F. Fercher, *Opt. Express* **11**, 889 (2003). doi:[10.1364/OE.11.000889](https://doi.org/10.1364/OE.11.000889)
7. P. Targowski, M. Góra, M. Wojtkowski, *Laser Chem.* (2006). doi:[10.1155/2006/35373](https://doi.org/10.1155/2006/35373)
8. M. Iwanicka, L. Tymińska-Widmer, B. Rouba, E.A. Kwiatkowska, M. Sylwestrzak, P. Targowski, in *Proceedings of the International Conference LACONA VIII:—Lasers in the Conservation of Artworks*, ed. by R. Radvan, J.F. Asmus, M. Castilleo, P. Pouli, A. Nevin (CRC Press, Taylor & Francis Group, London, 2009), p. 209
9. M. Szkulmowski, M. Wojtkowski, P. Targowski, A. Kowalczyk, *Proc. SPIE* **5316**, 424 (2004). doi:[10.1117/12.529466](https://doi.org/10.1117/12.529466)
10. M. Pircher, E. Gotzinger, C.K. Hitzenberger, *J. Biomed. Opt.* **11**, 054013 (2006)
11. D. Woods, A. Podoleanu, *Opt. Express* **16**, 9654 (2008). doi:[10.1364/OE.16.009654](https://doi.org/10.1364/OE.16.009654)
12. American National Standard for Safe Use of Lasers: ANSI Z 136.1—2007 (Laser Institute of America, Orlando, 2007)
13. M.L. Yang, C.W. Lu, I.J. Hsu, C.C. Yang, *Archaeometry* **46**, 171 (2004). doi:[10.1111/j.1475-4754.2004.00151.x](https://doi.org/10.1111/j.1475-4754.2004.00151.x)
14. H. Liang, M. Cid, R. Cucu, G. Dobre, A. Podoleanu, J. Pedro, D. Saunders, *Opt. Express* **13**, 6133 (2005). doi:[10.1364/OPEX.13.006133](https://doi.org/10.1364/OPEX.13.006133)
15. F.T. Arecchi, M. Bellini, C. Corsi, R. Fontana, M. Materazzi, L. Pezzati, A. Tortora, *Optical coherence tomography for painting diagnostics. Proc. SPIE* **5857**, 58570Z (2005). doi:[10.1117/12.612558](https://doi.org/10.1117/12.612558). *Optical Methods for Arts and Archaeology*
16. M.-L. Yang, A.M. Winkler, J.K. Barton, P.B. Vandiver, *Archaeometry* **51**, 808 (2009). doi:[10.1111/j.1475-4754.2008.00451.x](https://doi.org/10.1111/j.1475-4754.2008.00451.x)
17. M. Hughes, PhD thesis, University of Kent in Canterbury (2010), http://www.mike-hughes.org/files/phd_oct_for_art.pdf accessed: 31.03.2011
18. P. Targowski, M. Iwanicka, L. Tymińska-Widmer, M. Sylwestrzak, E.A. Kwiatkowska, *Acc. Chem. Res.* **46**, 826 (2010). doi:[10.1021/ar900195d](https://doi.org/10.1021/ar900195d)
19. D.C. Adler, J. Stenger, I. Gorczynska, H. Lie, T. Hensick, R. Spronk, S. Wolohojian, N. Khandekar, J.Y. Jiang, S. Barry, *Opt. Express* **15**, 15972 (2007). doi:[10.1364/OE.15.015972](https://doi.org/10.1364/OE.15.015972)
20. M. Hughes, D.A. Jackson, A.G. Podoleanu, *Proc. SPIE* **7139**, 713917 (2008). doi:[10.1117/12.816222](https://doi.org/10.1117/12.816222)
21. S. Chang, Y. Mao, C. Flueraru, G. Chang, *Opt. Eng.* **49**, 063602 (2010). doi:[10.1117/1.3449112](https://doi.org/10.1117/1.3449112)
22. G. Latour, J. Moreau, M. Elias, J.-M. Frigerio, *Proc. SPIE* **6618**, 661806 (2007). doi:[10.1117/12.726084](https://doi.org/10.1117/12.726084)
23. G. Latour, G. Georges, L. Siozade, C. Deumié, J.-P. Echard, *Proc. SPIE* **7391**, 73910J (2009). doi:[10.1117/12.827856](https://doi.org/10.1117/12.827856)
24. G. Latour, J.P. Echard, B. Soulier, I. Emond, S. Vaiedelich, M. Elias, *Appl. Opt.* **48**, 6485 (2009)
25. I. Gurov, A. Karpets, N. Margariants, E. Vorobeve, *Proc. SPIE* **6618**, 661807 (2007). doi:[10.1117/12.726315](https://doi.org/10.1117/12.726315)
26. M. Góra, M. Pircher, E. Göttinger, T. Bajraszewski, M. Strlic, J. Kolar, C.K. Hitzenberger, P. Targowski, *Laser Chem.* (2006). doi:[10.1155/2006/68679](https://doi.org/10.1155/2006/68679)
27. M. Hughes, M. Spring, A. Podoleanu, *Appl. Opt.* **49**, 99 (2010)
28. M. Sylwestrzak, E.A. Kwiatkowska, P. Karaszkiwicz, M. Iwanicka, P. Targowski, *Proc. SPIE* **7391**, 739109 (2009). doi:[10.1117/12.827520](https://doi.org/10.1117/12.827520)

29. M. Sylwestrzak, M. Szkulmowski, D. Szlag, P. Targowski, *Photonics Lett. Pol.* **2**, 137 (2010). doi:[10.4302/plp.2010.3.14](https://doi.org/10.4302/plp.2010.3.14)
30. H. Liang, R. Cucu, G. Dobre, D.A. Jackson, J. Pedro, C. Pannell, D. Saunders, A.G. Podoleanu, *Proc. SPIE* **5502**, 378 (2004). doi:[10.1117/12.566780](https://doi.org/10.1117/12.566780)
31. Complete list of papers on application of OCT to examination of artwork (2011), <http://www.oct4art.eu> accessed: 31.03.2010
32. T. Arecchi, M. Bellini, C. Corsi, R. Fontana, M. Materazzi, L. Pezzati, A. Tortora, *Opt. Spectrosc.* **101**, 23 (2006). doi:[10.1134/S0030400X06070058](https://doi.org/10.1134/S0030400X06070058)
33. A. Szkulmowska, M. Góra, M. Targowska, B. Rouba, D. Stifter, E. Breuer, P. Targowski, in *Lasers in the Conservation of Artworks, LACONA VI Proceedings*, Vienna, Austria, Sept. 21–25, 2005, ed. by J. Nimmrichter, W. Kautek, M. Schreiner (Springer, Berlin-Heidelberg-New York, 2007), p. 487
34. H. Liang, B. Peric, M. Hughes, A. Podoleanu, M. Spring, D. Saunders, *Proc. SPIE* **6618**, 661805 (2007). doi:[10.1117/12.726032](https://doi.org/10.1117/12.726032)
35. H. Liang, M. Cid, R. Cucu, G. Dobre, B. Kudimov, J. Pedro, D. Saunders, J. Cupitt, A. Podoleanu, *Proc. SPIE* **5857**, 261 (2005). doi:[10.1117/12.612591](https://doi.org/10.1117/12.612591)
36. E.R. de la Rie, *Stud. Conserv.* **32**, 1 (1987)
37. H. Liang, B. Peric, M. Hughes, A.G. Podoleanu, M. Spring, S. Roehrs, Optical coherence tomography in archaeological and conservation science—a new emerging field. *Proc. SPIE* **7139**, 713915 (2008). doi:[10.1117/12.819499](https://doi.org/10.1117/12.819499). 1st Canterbury Workshop on Optical Coherence Tomography and Adaptive Optics
38. M. Spring, H. Liang, B. Peric, D. Saunders, A. Podoleanu, in *Proceedings of ICOM-CC Triennial Conference*, vol. II—Preprints (Allied, New Delhi, 2008), p. 916
39. B. Rouba, P. Karaszkiwicz, L. Tymińska-Widmer, M. Iwanicka, M. Góra, E. Kwiatkowska, P. Targowski, presented at the *9th International Conference on Non Destructive Testing of Art*, Jerusalem, Israel, May 25–30, 2008 (e-Journal of NDT, 2008), <http://www.ndt.net/search/docs.php3?MainSource=-1&id=6014> accessed: 31.03.2011
40. M. Dupont, K. Hinrichs, in *Proceedings of ICOM-CC 8th Triennial Meeting*, ed. by K. Grimstad, vol. 3 (Getty Conservation Institute, Sydney, 1987), p. 957
41. P. Targowski, P. Karaszkiwicz, B.J. Rouba, D. Markowski, L. Tymińska-Widmer, M. Iwanicka, E.A. Kwiatkowska, M. Sylwestrzak, in *The Art of Collaboration: Stained-Glass Conservation in the Twenty-First Century*, ed. by M.B. Shepard, L. Pilosi, S. Strobl (Brepols, Turnhout, 2010), p. 127. Corpus Vitrearum USA, Occasional Papers II
42. P. Targowski, B. Rouba, M. Góra, L. Tymińska-Widmer, J. Marczak, A. Kowalczyk, *Appl. Phys. A* **92**, 1 (2008). doi:[10.1007/s00339-008-4446-x](https://doi.org/10.1007/s00339-008-4446-x)
43. J. Kunicki-Goldfinger, P. Targowski, M. Góra, P. Karaszkiwicz, P. Dzierżanowski, *Stud. Conserv.* **54**, 117 (2009)
44. C. Fotakis, D. Anglos, V. Zafiropoulos, S. Georgiu, V. Tornari, *Lasers in the Preservation of Cultural Heritage* (CRC Press, Boca Raton, 2007), p. 53
45. V. Detalle, M. Dufour, J.-P. Monchalain, M. Sabsabi, L. St-Onge, US Patent 6,873,419, 2005
46. M.L. Dufour, G. Lamouche, V. Detalle, B. Gauthier, P. Sammut, *Insight* **47**, 216 (2005). doi:[10.1784/insi.47.4.216.63149](https://doi.org/10.1784/insi.47.4.216.63149)
47. D.G. Papazoglou, V. Papadakis, A. Demetrios, *J. Anal. At. Spectrom.* **19**, 483 (2004)
48. M.M. Amaral, M.P. Raelle, A.Z. de Freitas, G.S. Zahn, R.E. Samad, N.D. Vieira, L.V.G. Tarelho, *Proc. SPIE* **7391**, 73910J (2009). doi:[10.1117/12.827724](https://doi.org/10.1117/12.827724)
49. E.A. Kwiatkowska, J. Marczak, R. Ostrowski, W. Skrzeczanowski, M. Sylwestrzak, M. Iwanicka, P. Targowski, *Proc. SPIE* **7391**, 73910J (2009). doi:[10.1117/12.827271](https://doi.org/10.1117/12.827271)
50. P. Targowski, E.A. Kwiatkowska, M. Sylwestrzak, J. Marczak, W. Skrzeczanowski, R. Ostrowski, E. Szmit-Naud, M. Iwanicka, in *Proceedings of the International Conference LACONA VIII:—Lasers in the Conservation of Artworks*, ed. by R. Radvan, J.F. Asmus, M. Castilleo, P. Pouli, A. Nevin (CRC Press, Taylor & Francis Group, London 2009), p. 143
51. Final Report CRAFT project ENV4-CT98-0787 (2011), http://www.art-innovation.nl/fckfiles/file/Downloads/Articles/2001/2001b_advanced_workstation_final_report.pdf accessed: 31.03.2011
52. M. Góra, A. Rycyk, J. Marczak, P. Targowski, A. Kowalczyk, *Proc. SPIE* **6429**, 64292V (2007). doi:[10.1117/12.703333](https://doi.org/10.1117/12.703333)
53. M. Góra, P. Targowski, A. Kowalczyk, J. Marczak, A. Rycyk, in *Lasers in the Conservation of Artworks, LACONA VII Proceedings*, ed. by M. Castilleo. Madrid, Spain, Sept. 17–21, 2007 (Taylor & Francis Group, London, 2008), p. 23
54. P. Targowski, R. Ostrowski, J. Marczak, M. Sylwestrzak, E.A. Kwiatkowska, *Proc. SPIE* **7391**, 739115 (2009). doi:[10.1117/12.827286](https://doi.org/10.1117/12.827286)
55. P. Targowski, M. Góra, J. Marczak, A. Rycyk, B.J. Rouba, *SPIE Newsroom* (2009). doi:[10.1117/2.1200904.1589](https://doi.org/10.1117/2.1200904.1589)